

Texture Evolution During Cross Rolling and Annealing of High-Purity Nickel

PINAKI PRASAD BHATTACHARJEE, M. JOSHI, V.P. CHAUDHARY, J.R. GATTI, and M. ZAID

Evolution of texture during cross rolling and subsequent annealing was studied in high-purity nickel. For this purpose nickel samples were subjected to multipass cross rolling up to 90 pct reduction in thickness followed by annealing at different temperatures ranging between 673 K and 1073 K (400 °C and 800 °C). Cross rolling was carried out by rotating the samples about the normal direction (ND) by 90 deg interchanging the rolling direction and transverse direction (TD) between each consecutive pass. The development of microstructure and texture was characterized using X-ray and electron backscattered diffraction (EBSD) techniques. The deformation texture was characterized by the presence of strong brass ($\{110\}\langle 112\rangle$) and ND-rotated brass ($\{011\}\langle 21\bar{1}313\rangle$) orientations. Upon annealing at 673 K (400 °C), ND \parallel [111] fiber could be observed in the microtexture which originated from the twin formation of the recrystallized TD-rotated cube ($\{027\}\langle 072\rangle$) grains. The fiber was weakened after annealing at 1073 K (800 °C) because of the decreased propensity for twin formation, and the microtexture was found to be weak and diffused. EBSD studies on early recrystallization stages indicated the absence of preferential nucleation of cube grains being in agreement with a weak cube texture formation in annealed cross-rolled high-purity nickel.

DOI: 10.1007/s11661-013-1617-y

© The Minerals, Metals & Materials Society and ASM International 2013

I. INTRODUCTION

DEFORMATION processing of materials by cold rolling is usually accompanied by the development of characteristic microstructure and crystallographic texture, which in turn influences the development of recrystallization texture during subsequent annealing.^[1] In high-to-medium stacking fault energy face-centered-cubic (fcc) materials, the cold-rolling texture is described by pure metal- or copper-type texture characterized by the presence of strong Cu ($\{112\}\langle 111\rangle$), S ($\{123\}\langle 634\rangle$), and brass (B_S , $\{110\}\langle 112\rangle$) orientations. In contrast, the low stacking fault energy materials are found to develop alloy- or brass-type texture where the B_S orientation becomes the dominant texture component, while the S or Cu components are diminished in strength.^[2,3] With increasing stacking fault energy, a gradual transition of

texture from pure metal- or copper-type texture to prominent alloy- or brass-type texture is observed.^[3,4] The development of texture in fcc metals may also be conveniently described by the intensity distribution along two incomplete fibers: α fiber which runs from the Goss orientation ($\{110\}\langle 001\rangle$), to the B_S orientation ($\{110\}\langle 112\rangle$); and the β -fiber which extends from the Cu orientation to the B_S orientation through the S-orientation.

However, the processing parameters, such as change in strain path,^[5,6] difference in roll velocities such as asymmetric rolling,^[7] and rolling temperature,^[8] can affect the development of texture, and a deviation from the above simplistic description of texture formation is observed. Among several processing parameters the strain path change during cold rolling is found to significantly affect the evolution of deformation texture.^[5,6] The strain path change during cold rolling can be implemented by adopting the cross-rolling procedure in which the sample is rotated about the normal direction (90 deg) between the consecutive passes so that the rolling and transverse direction (RD and TD, respectively) are mutually interchanged in each pass.^[5]

Cross rolling is found to affect the microstructure and texture formation during deformation processing and annealing to a significant extent, which has been extensively studied in various aluminum and copper alloys.^[9–13] In contrast, the cross-rolling texture of nickel has been studied only to a limited extent. It has recently been observed by Gurao *et al.*^[13] that cross-rolled high-purity nickel develops a cold rolling texture dominated by B_S and ND rotated- B_S components.

PINAKI PRASAD BHATTACHARJEE, Assistant Professor, J.R. GATTI, and M. ZAID, PhD students, are with the Department of Materials Science and Engineering, Indian Institute of Technology Hyderabad, Ordnance Factory Campus, Yeddumailaram 502205, Andhra Pradesh, India. Contact e-mail: pinakib@iith.ac.in M. JOSHI, formerly MTech Student, with the Department of Materials Science and Engineering, Indian Institute of Technology Hyderabad, is now PhD student with the Department of Materials Science and Engineering, Graduate School of Engineering, Yoshida, Honmachi, Sakyo-Ku, Kyoto 606-8501, Japan. V.P. CHAUDHARY, formerly MTech Student, with the Department of Materials Science and Engineering, Indian Institute of Technology Hyderabad, is now Lecturer, with the Department of Materials Science and Engineering, Rajiv Gandhi University of Knowledge Technologies, Hyderabad, India.

Manuscript submitted June 18, 2012.

Article published online January 31, 2013

Interestingly, sharp cube texture formation is not observed in heavily cross-rolled and annealed materials, although, more cube-oriented regions could be observed in the deformed microstructure.^[11,12,14] This is in stark contrast to the recrystallization texture of heavily straight-rolled medium-to-high stacking fault energy fcc materials where strong cube texture formation is widely reported.^[1,15] Such differences in the formation of recrystallization texture in cross-rolled materials have been discussed in the context of pertinent theories of formation of recrystallization texture, namely, oriented nucleation and oriented growth.^[11] Other models have also been proposed more recently to account for the origin of recrystallization texture of cross-rolled copper.^[14]

In the current study, we report the evolution of texture during heavy cross rolling and subsequent annealing of high-purity nickel which has been studied to a very limited extent, although, the texture evolution after uniaxial/straight rolling and annealing has been extensively studied because of the possible use of highly cube-textured nickel and nickel-based alloys for use as coated superconductor substrates.^[16,17] It is envisaged that the understanding of texture development during cross rolling and annealing nickel will be also helpful to understand the origin of cross-rolling texture in other fcc materials.

II. EXPERIMENTAL METHODS

A. Material Processing

In the current study, as-received Ni slab (~99.7 pct) having dimensions $\sim 160 \text{ mm}^L \times 60 \text{ mm}^W \times 10 \text{ mm}^T$ were deformed up to 50 pct reduction in thickness by multipass cold rolling followed by annealing at 823 K (550 °C) for 1 hour in a salt bath furnace. The temperature and time for annealing were chosen to achieve a weaker starting recrystallization texture and in addition relatively small recrystallized grain size. These fully recrystallized materials were used as the starting materials for further processing by multipass cross cold rolling (CCR). The fully recrystallized material was deformed up to ~90 pct reduction in thickness in steps of ~20, 40, 65, and 90 pct reductions using the multipass CCR processing route. Each deformation stage was reached in a single pass, and the RD and TD were interchanged between consecutive passes resulting in two straight and two transverse passes. Finally, the 90 pct CCR-processed sheets were subjected to isochronal annealing treatment for 1 hour in a salt bath furnace maintained at 673 K and 1073 K (400 °C and 800 °C), respectively. In order to study the early stages of recrystallization, a few specimens were annealed at 623 K (350 °C) for 10 seconds in the salt bath furnace.

B. Characterization

The microstructure and texture of the 20 pct (low strain), 65 pct (medium strain), and 90 pct (heavily strained) deformed materials were characterized at

different length scales using X-ray and electron back-scattered diffraction (X-ray diffraction (XRD) and EBSD, respectively) techniques. The bulk texture analysis of the samples was done using XRD technique in a Panalytical MRD system using Cu-K α radiation (1.54 Å). Four incomplete pole figures {200}, {220}, {111}, and {311} were measured, and the orientation distribution function (ODF) was calculated using the MTM-FHM software developed at KU Leuven, Belgium.^[18] The samples for bulk texture measurement by XRD were prepared by mechanical polishing using colloidal silica. The microstructure and microtexture of the deformed materials were characterized by fully automated EBSD system attached to a scanning electron microscope (SEM) equipped with field emission gun (FEI, Quanta 3D FEG). The TSL-OIM™ microtexture analysis software was used for the analysis of the microtexture data. The samples for microtexture measurement were prepared by careful mechanical polishing followed by electro-polishing at room temperature using a mixture of acetic and perchloric acids (10:1 ratio by volume) as electrolyte. A cut-off angle of 15 deg around the respective ideal locations was used for calculating the volume fractions of different texture components.

III. RESULTS

Figure 1 shows the grain boundary (GB) map fully recrystallized microstructure of the starting material used for the CCR processing. The high (HAGBs with

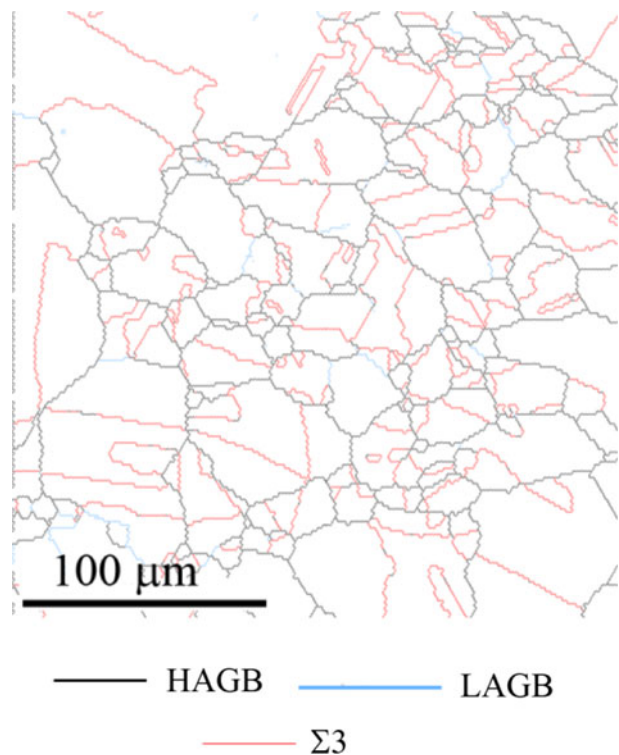


Fig. 1—GB map showing microstructure of the starting material for CCR processing.

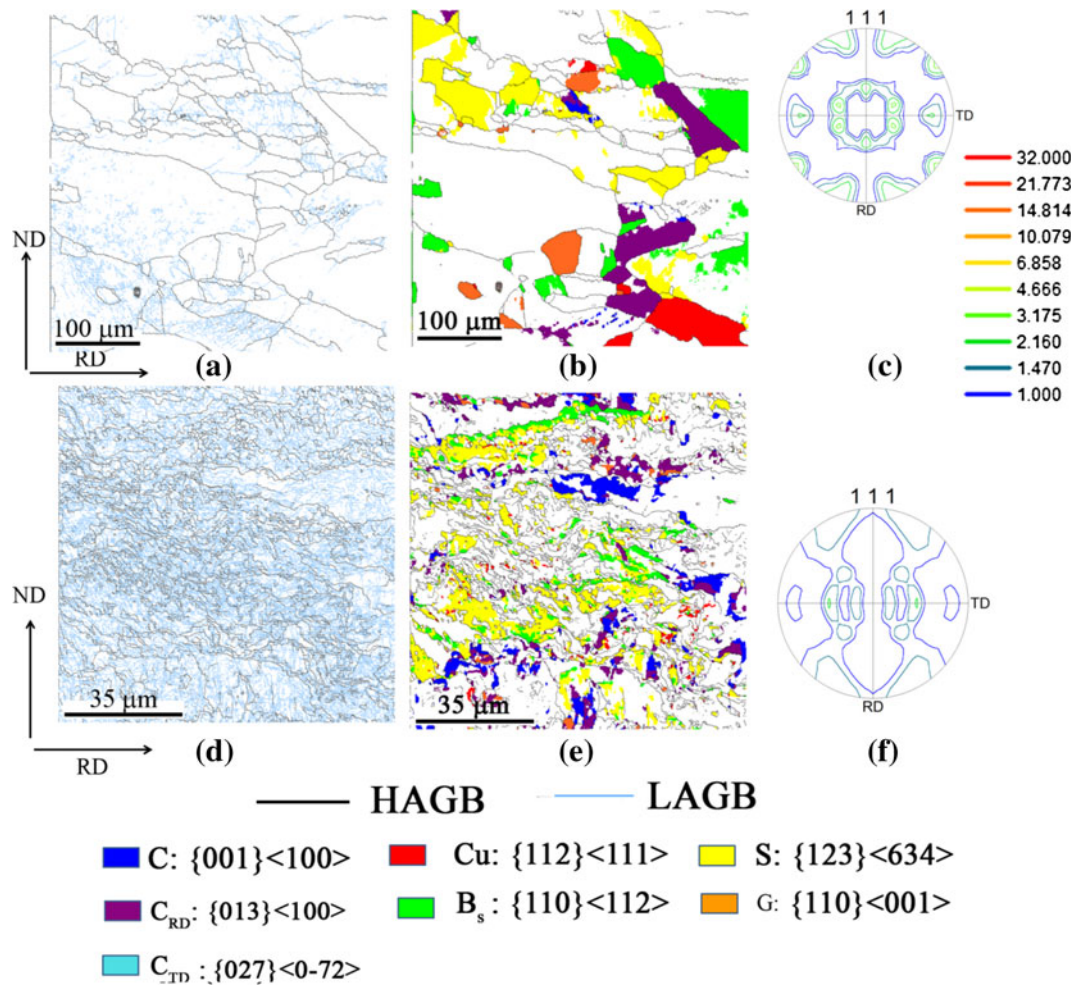


Fig. 2—(a) through (c) are the GB map, orientation map, and (111) PF of the 20 pct deformed materials. (d) through (f) are the GB map, orientation map, and (111) PF for the 65 pct cross-rolled material.

misorientation angle $\theta > 15$ deg) and low (LAGBs defined by $2 \text{ deg} \leq \theta \leq 15 \text{ deg}$) angle, and $\Sigma 3$ annealing twin boundaries have been highlighted in black, light blue, and red lines, respectively, in the GB map (this color convention for different grain boundaries are followed throughout this article). The average grain size in the recrystallized condition is $\sim 36 \mu\text{m}$. The texture of the material in this condition is found to be rather weak.

Figure 2 shows the gradual development of microstructure and texture with the increasing strain during cross rolling of the experimental materials. The microstructure after 20 pct deformation (Figure 2(a)) resembles the starting recrystallized microstructure, but inside the starting recrystallized grains, LAGB network could be clearly observed indicating the development of typical cell structure. The orientation map (Figure 2(b)) and the (111) pole figure (PF) (Figure 2(c)) indicate that the texture in this condition is rather weak. The microstructure (Figure 2(d)) following cross rolling to 65 pct reduction in thickness appears as a mixture of regions having deformed, coarse-banded structure elongated along the RD, and regions having rather fragmented structure. The orientation map (Figure 2(e)) shows the presence of fragmented and isolated S

(highlighted in yellow), B_S (highlighted in green), cube component (denoted by C; $\{001\}\langle 100\rangle$; highlighted in blue), and RD-rotated cube (denoted by C_{RD} ; $\{013\}\langle 100\rangle$; highlighted in purple)-oriented regions. Random fraction is found to be quite high in this condition. The orientation map together with the (111) PF (Figure 2(f)) reveals rather weak deformation texture present in this condition.

Figure 3 shows the bulk texture of 90 pct deformed material obtained by XRD. A comparison of the (111) PF (Figure 3(a)) with the ideal (111) PF (Figure 3(b)) clearly shows that strong intensity is present around the B_S location indicating the development of a strong B_S texture in this deformed condition. This is further corroborated from the $\varphi_2 = 0$ deg section of the ODF (Figure 3(c)) which shows strong intensity maxima close to the ideal B_S location ($(\varphi_1, \varphi, \text{ and } \varphi_2) = (35.3, 45, \text{ and } 0 \text{ deg})$). Further analysis shows that the local intensity maxima associated with the B_S orientation is slightly shifted along the φ_1 axis from the ideal B_S orientation and located at $(\varphi_1, \varphi, \text{ and } \varphi_2) = (41.3, 45, \text{ and } 0 \text{ deg})$ which correspond to an ND-rotated B_S orientation (B_S^{ND}) denoted by (01 1) $[21 \bar{1}3 13]$ having a misorientation of ~ 6 deg around $[101]$ axis.

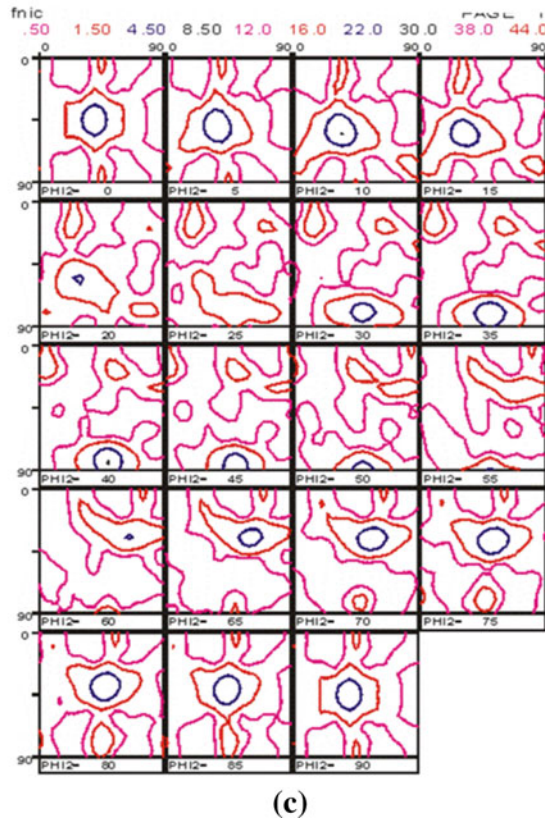
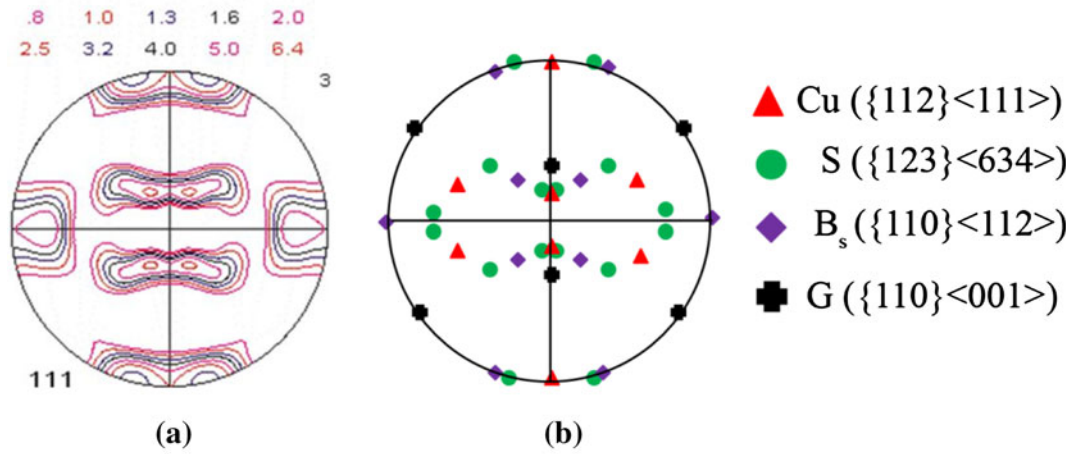


Fig. 3—(a) the (111) PF of 90 pct cross-rolled nickel and (b) the ideal locations of typical deformation texture components in a (111) PF. (c) the ODF.

Figure 4 shows the microstructure and microtexture of the 90 pct deformed material obtained from two different regions using EBSD. Figure 4(a) shows the image quality (IQ) map of a region of interest which shows some interesting features of the deformed material. Very thin, long, and intersecting shear bands (indicated by the arrow marks) inclined to the RD by ~26 to 30 deg could be observed. Another interesting feature observed in the IQ map is the appearance of an intense, locally sheared region (shown enclosed by the broken circle) with decidedly much finer microstructure than the bulk which also possibly shows a shear vortex. The corresponding orientation map (Figure 4(b)) reveals the presence of C (blue), C_{RD} (purple), and

TD-rotated cube (denoted by C_{TD} ; $\{027\}\{0\bar{7}2\}$; aqua) orientations in this locally sheared region. In contrast, away from this sheared region, the microtexture is dominated mainly by the B_S (green, ~8.2 pct) and B_S^{ND} (pale green; ~14.4 pct), and S component. The (111) PF (Figure 4(c)) also reveals the strong presence of the B_S component. Since the volume fraction of the B_S^{ND} component is more than the B_S component, this results in the shift of the intensity maxima toward the B_S^{ND} location which is clearly evidenced from the $\varphi_2 = 0$ deg section of the ODF (Figure 4(d)).

Figures 4(e) and (f) show the GB and orientation maps, respectively, obtained from another region in the 90 pct deformed material. The maps reveal a rather

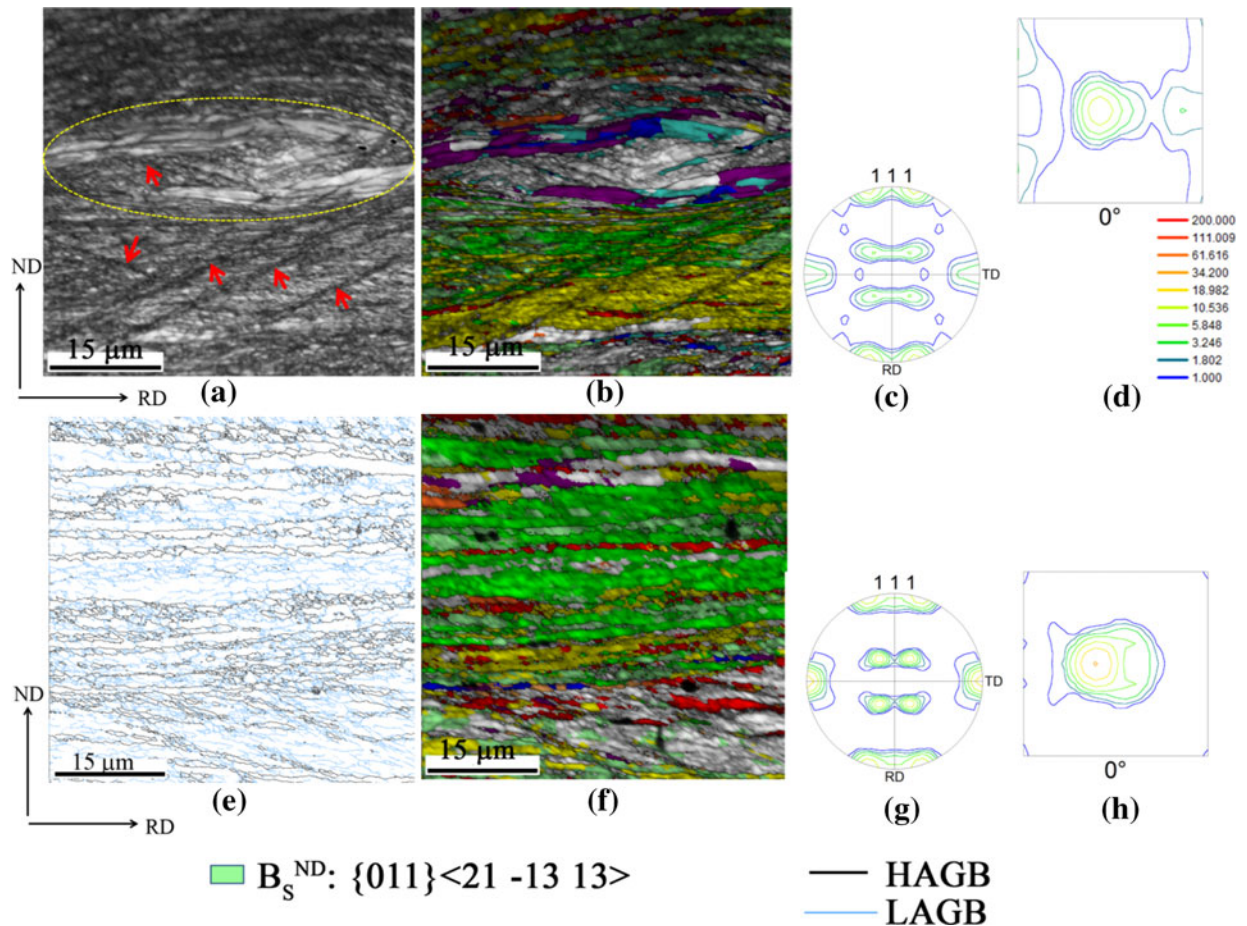


Fig. 4—(a) through (d) are IQ map, orientation map, (111) PF, and $\varphi_2 = 0$ deg section of the ODF of 90 pct cross-rolled material; (e) through (h) are the GB map, orientations map, (111) PF, and $\varphi_2 = 0$ deg section of the ODF obtained from another region of the same material. The color codes for the orientations are the same as in Fig. 2 except for the B_S^{ND} orientation shown in this figure.

lamellar structure subdivided by HAGBs along the ND typical of heavily deformed fcc materials. The orientation map clearly shows the presence of very strong B_S (green, ~30.4 pct) and B_S^{ND} (pale green, ~16.2 pct) components which are also clearly observed from the (111) PF (Figure 4(g)). As the B_S component is stronger than the B_S^{ND} component in this region, the local intensity maxima as a result are found closer to the ideal B_S location as were also observed in the $\varphi_2 = 0$ deg section of the ODF (Figure 4(h)).

Figure 5 shows the microstructure and texture development in the 90 pct deformed material following annealing at 673 K (400 °C) for 1 hour. Very interestingly, the (111) PF (Figure 5(a)) of the 673 K (400 °C)-annealed specimen shows the development of a ND||{111} fiber texture. The development of such an unusual ND fiber texture is clearly understood from the $\varphi_2 = 45$ deg section of the ODF (Figure 5(b)) where the ideal (111) fiber is shown in dotted line along with the locations of several ideal orientations on this fiber using different symbols. However, the intensity distribution along the fiber is not uniform, and local intensity maxima are located at $(\varphi_1, \varphi, \text{ and } \varphi_2) = (0, 55, \text{ and } 45 \text{ deg})$ corresponding to the orientation (111)[1 $\bar{1}$ 0] (shown by square) and $(\varphi_1, \varphi, \text{ and } \varphi_2) = (23, 49, \text{ and } 45 \text{ deg})$ (shown by the inverted triangle symbol) corresponding to the orientation (445)[13 $\bar{2}$ 38].

45 deg) (shown by the inverted triangle symbol) corresponding to the orientation (445)[13 $\bar{2}$ 38].

The quantitative analysis of the texture development in the annealed condition could be done from the corresponding orientation map shown in Figure 5(c). The presence of the fiber orientations observed from the PF and the ODF analyses is amply corroborated from the orientation map (Figure 5(c)). The volume fractions of the two ND||{111} fiber orientations (111)[1 $\bar{1}$ 0] (dark yellow) and (445)[13 $\bar{2}$ 38] (pink) are found to be ~12 and 9.4 pct, respectively. The volume fraction of the C component is quite small (~1.7 pct), but the presence of the C_{TD} (aqua) component is noticed having a volume fraction of ~6.2 pct. Remarkably, the grains with the fiber orientation (445)[13 $\bar{2}$ 38] are mostly found adjacent to the C_{TD} orientation separated by the $\Sigma 3$ annealing twin boundaries (highlighted by red lines) which have been highlighted by broken circles for clarity. This indicates that (445)[13 $\bar{2}$ 38] oriented originates from the twin formation of the C_{TD} and henceforth denoted as C_{TD}^T (i.e., twin of the C_{TD}). The C_{TD}^T grain shown by the block arrow has the same orientation as the two small twin grains in the adjacent parent C_{TD} grain shown by thin arrow. The volume fraction of the dominant deformation texture components such as B_S (green;

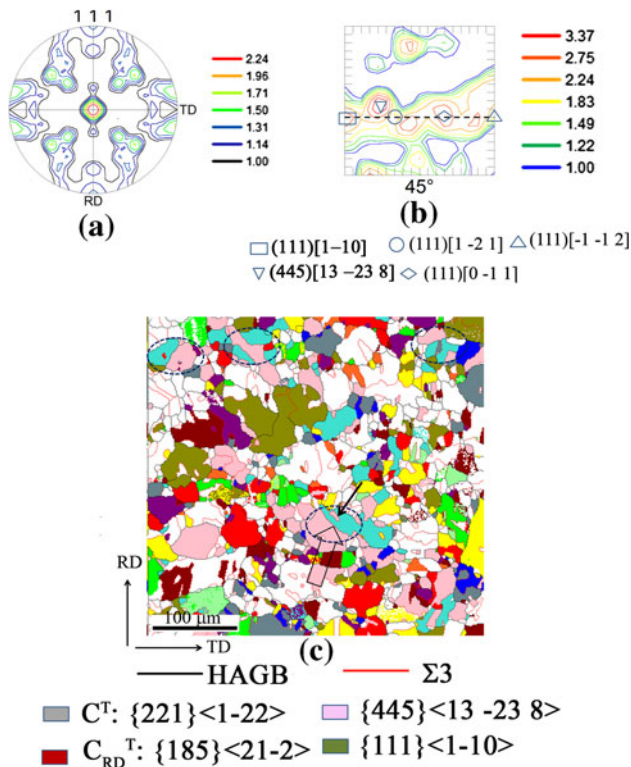


Fig. 5—(a) (111) PF, (b) ODF, and (c) orientation map of nickel after 90 pct cross rolling and annealing at 673 K (400 °C). The color codes for the orientations are the same as in Figs. 2 and 4 except for the orientations shown separately in this map.

~3.5 pct) and B_S^{ND} (light green; 1.9 pct) are significantly diminished in strength in this annealed condition.

Figure 6 shows the microstructure and texture development upon high-temperature annealing treatment at 1073 K (800 °C) for 1 hour. The orientation map of 1073 K (800 °C) (Figure 6(a)) shows the presence of the few large C_{TD} -oriented regions (aqua), and the volume fraction, although it increases in comparison with the 673 K (400 °C), still is rather low ~12 pct. The presence of the C_{TD} orientation is corroborated from the corresponding (111) PF (Figure 6(b)) and $\phi_2 = 0$ deg section of the ODF (Figure 6(c)). The fiber observed in the 673 K (400 °C)-annealed specimen becomes weaker which may be clearly understood by comparing the intensities of the contours of around the central location of (111) PF of the 1073 K (800 °C) (Figure 6(b)) and the $\phi_2 = 45$ deg section (Figure 6(c)) with those of the 673 K (400 °C) specimen (Figures 5(a) and (b)). The two fiber orientations observed in the 673 K (400 °C)-annealed specimen, *i.e.*, (111)[1 $\bar{1}$ 0] and (445)[13 $\bar{2}$ 38] are lower in strength after annealing at 1073 K (800 °C), and their volume fractions are found to be ~2.0 and 6 pct, respectively.

Figures 7(a) and (b) show the grain boundary character distribution (GBCD) and coincidence site lattice (CSL) boundary distribution, respectively, in the two annealed conditions. Nearly four hundred recrystallized grains have been analyzed to obtain the presented data. The LAGB fraction remains almost similar in the two annealed conditions. However, the 673 K (400 °C)-

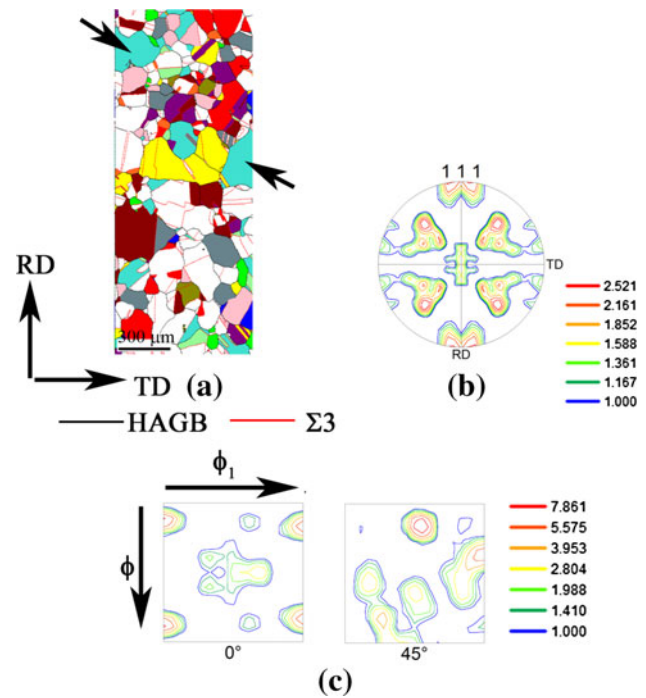


Fig. 6—(a) Orientation map, (b) (111) PF and (c) $\phi_2 = 0$ deg and $\phi_2 = 45$ deg section of the ODF of nickel after 90 pct cross rolling and annealing at 1073 K (800 °C). The color codes for the orientations are the same as in Figs. 2 through 5.

annealed specimen shows much higher CSL fraction (~0.57) and lower HAGB fraction (~0.40) as compared with the 1073 K (800 °C)-annealed specimen where the CSL and HAGB fractions are found to be 0.49 and 0.47, respectively. The CSL distribution (Figure 7(b)) in both the annealed conditions clearly indicates that most of the CSL boundaries have $\Sigma 3$ character. The fraction of $\Sigma 3$ boundaries is decidedly larger in the 673 K (400 °C) (~0.47)-annealed specimen as compared with the 1073 K (800 °C) (~0.42)-annealed specimen.

The volume fractions of different texture components in deformed and annealed conditions are summarized in Table I for the easy and clear understanding of the discussion that follows.

IV. DISCUSSION

A. Evolution of Deformation Texture

The straight rolling texture of pure nickel can be adequately described by the gradual evolution of a strong β fiber texture which is characterized by usually strong C_u , S , and B_S components.^[2] In contrast, in the studied case, the deformation texture during CCR processing gradually strengthens with the increasing thickness reduction and is characterized by the strong B_S and B_S^{ND} orientations in heavily deformed condition. It might be noted that such strong B_S and rotated brass texture due to CCR processing has also been reported previously in nickel, copper, and copper alloys.^[13,14,19]

The origin of deformation texture during deformation processing has been discussed from the view point of

stability of different orientations in terms of the rotation field $\dot{R}(\dot{\varphi}_1, \dot{\varphi}, \dot{\varphi}_2)$ and the divergence of the rotation field $(\text{div } \dot{R} = \frac{\partial \dot{\varphi}_1}{\partial \varphi_1} + \frac{\partial \dot{\varphi}}{\partial \varphi} + \frac{\partial \dot{\varphi}_2}{\partial \varphi_2})$.^[20,21] The stability conditions are then given by $\dot{R} = 0$ and $\text{div}(\dot{R}) = 0$. The theoretical calculations of Hong *et al.*^[14] predict that among different texture components, the $\{011\}\langle 1\bar{1}1 \rangle$ (which is basically ND rotated B_S orientation) would be

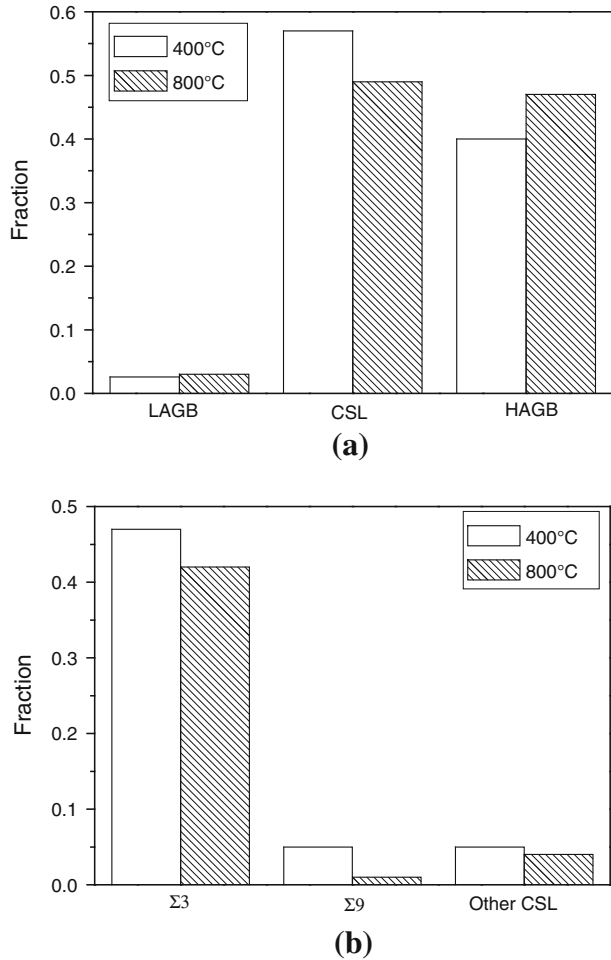


Fig. 7—(a) GBCD and (b) CSL distribution of 90 pct cross-rolled and annealed nickel.

stable under cross rolling because of its higher inverse rotation rate and large negative divergence. The grains with orientations along the α -fiber will rotate to the B_S orientation (stable orientation during unidirectional rolling and then will further rotate away to the $\{011\}\langle 1\bar{1}1 \rangle$ orientation when the direction of rolling is changed by 90 deg around the ND, thus, oscillating between the B_S and rotated brass orientation $\{011\}\langle 1\bar{1}1 \rangle$ which would be the two stable end orientations in CCR. These theoretical calculations agree well with their experimental results which show strong $\{011\}\langle 755 \rangle$ orientation as the main component of deformation texture and spread around these orientations because of the oscillation between the two predicted stable end orientations. In the present case, the strongest texture components as observed both from microtexture and bulk texture measurements are the B_S and B_S^{ND} orientation $(011)[21\bar{1}3]$ which is in fact very close to the orientation $\{011\}\langle 755 \rangle$. The current experimental results thus agree quite well with the theoretical and experimental observations of Hong *et al.*

Previous investigations on CCR-processed materials have shown the development of cube orientation as a minor texture component alongside the major component.^[11,12,14] Although development of cube texture is ruled out in the present case from the microtexture and bulk texture results, isolated cube-oriented regions in form of thin bands are clearly observed in the vicinity of locally sheared region in the EBSD map with characteristic spread around RD and TD. Evidently, the volume fraction of the cube component is rather small, and as a result, it is not immediately apparent in the PFs and ODFs.

B. Evolution of Recrystallization Texture

Although the deformed material showed thin cube-oriented regions, in the recrystallization texture cube component appears rather weak. Instead, the development of a ND|| $\langle 111 \rangle$ fiber microtexture after annealing is observed after low-temperature annealing but after high-temperature annealing at 1073 K (800 °C) this texture is weakened. It may be noted this behavior is in contrast with the usual recrystallization texture of

Table I. Volume Fractions of the Texture Components in Different Cross-Rolled and Annealed Materials

Sample	Texture Components (Volume Percent)								
	Cube	Cu	S	B_S	G	B_S^{ND}	C_{RD}	C_{TD}	ND $\langle 111 \rangle$ Fiber C_{TD}^T (111) $\langle 1\bar{1}0 \rangle$
Deformed									
20 pct	0.4	3.2	9.3	6.5	2.2	—	5.7	—	—
65 pct	4.5	0.8	11.3	3.8					
90 pct									
Locally sheared region	1.5	3.9	24.6	8.2	1.0	14.4	8.1	5.2	—
Lamellar region	0.5	7.6	15.2	30.4	1.1	16.2	1.8	0.9	—
90 pct deformed and annealed									
673 K (400 °C)	1.7	5.7	6.4	3.5	1.2	1.9	4.1	6.2	12
1073 K (800 °C)	1.1	12.3	6.2	1.5	1.9	1.7	8.9	12.2	6.0

heavily cold rolled Ni where strong cube texture formation has been almost universally reported and the origin of such a sharp recrystallization texture has been discussed in terms of the two pertinent theories of formation of cube texture, namely, oriented nucleation and oriented growth depending up on the relative importance of the nucleation and growth stage on the formation of recrystallization texture.^[1,15]

The origin of the ND||[111] fiber texture can be understood by the spatial distribution of the (445)[13 $\bar{2}$ 38] in the microtexture map (Figure 5(c)) which shows that this component is found frequently adjacent to the TD oriented cube grains (027)[0 $\bar{7}$ 2] separated by Σ 3 annealing twin boundaries. This indicates that the origin of this orientation is the twin formation of the parent TD-oriented grains.

The propensity for annealing twin formation during recrystallization may be related to the growth stagnation. The growth stagnation may happen when the growing recrystallized grains are separated from the deformed matrix by low misorientation boundaries which has been demonstrated by in situ experiments.^[22] Occurrence of twin formation becomes favorable because twin formation can reorient the parent grains to alter the local misorientation so that growth can continue. The situation might be understood from the orientation map in Figure 5(c). The C_{TD}^T grain shown by block arrow has the same orientation as the two small twin grains in the adjacent parent C_{TD} grain. After the in situ EBSD observations of Field *et al.*^[22], it appears that the C_{TD}^T grain might have nucleated from the boundary of the parent C_{TD} grain because of the growth stagnation, and with progressing recrystallization, it has eventually become independent of the parent C_{TD} and thus finally appears as an independent grain in the microstructure.

To further elucidate this fact, the orientation map obtained after short-time annealing treatment (10 seconds at 623 K (350 °C)) is presented in Figure 8. The annealing temperature (623 K (350 °C)) and time (10 seconds) for partially recrystallized condition was established by trial and error method to yield only a few recrystallized grains. The recrystallized grains could be observed clearly in still-deformed matrix (masked in black) in Figure 8. The distribution of orientation is rather diverse but the presence of the C_{TD} grains are noticed along with recrystallized grains of other orientations. The early recrystallized C_{TD} grains are already found to be separated from its twin orientation C_{TD}^T by Σ 3 boundaries an example of which is shown by the arrow mark. It appears to be quite logical that this twinned grains grow independent of the parent grains finally giving rise to the observed ND||[111] fiber in the microtexture. It may be noted that the microtexture results of 673 K (400 °C)-annealed CCR-processed nickel bear resemblance to the recrystallization texture of cross-rolled copper which consists of a weak cube component and twin of the cube component as has been reported by Öztürk.^[12] Of course, in the studied case, rather than cube-oriented grains mostly C_{TD} and twin of this orientation are observed.

The weakening of this microtexture in high-temperature annealing appears to be also in agreement with the

decreased propensity for twin formation as clearly evidenced in the comparative GBCD plots of 673 K- and 1073 K (400 °C and 800 °C)-annealed conditions which shows significant decrease in the CSL fraction in the 1073 K (800 °C)-annealed condition because of the decrease in the Σ 3 annealing twin boundary fraction (Figure 7). The current results are in good agreement with those of Field *et al.*^[22] who observed that higher twin densities develop at lower annealing temperatures on the formation of annealing twins during recrystallization of Cu. It has been proposed that at higher annealing temperatures, the growth of the grains should be less dependent on twin formation as the thermal energy should be adequate to meet the required driving force. Thus, the newly recrystallized grains can grow free of hindrance. Support for this observation is obtained from the presence of large twin-free C_{TD} -oriented grains (shown by arrow marks) in the orientation map of 1073 K (800 °C)-annealed specimen (Figure 6(a)).

While the C_{TD}^T component originates from the twin formation of the recrystallized C_{TD} grains, no such definitive relations could be found for the (111)^[1-10] component from the orientation map of the 673 K (400 °C)-annealed specimen (Figure 5(c)) which indicates that this texture component might have originated from the usual nucleation and growth process during annealing. During high-temperature annealing, this component could possibly be consumed because of the

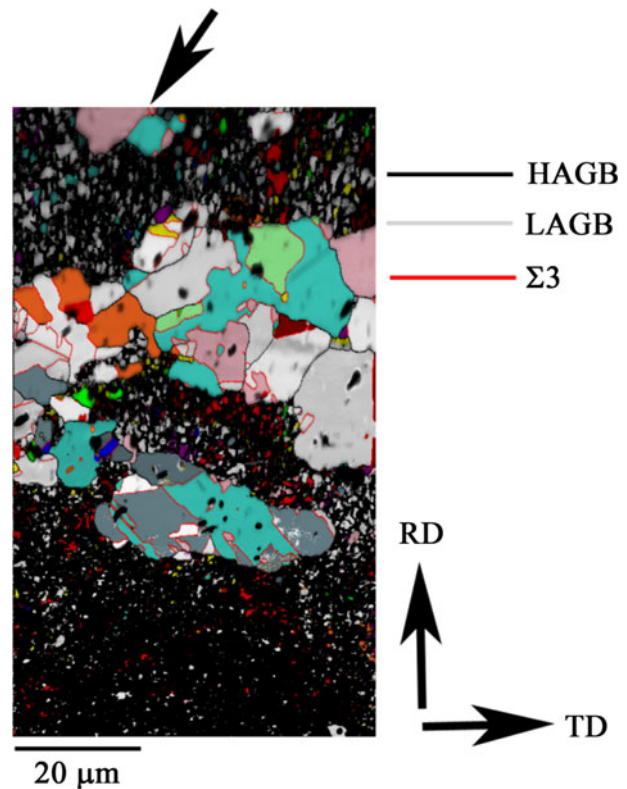


Fig. 8—Orientation map of 90 pct cross-rolled nickel after annealing at 623 K (350 °C) for 10 s showing recrystallized grains in still-deformed matrix (masked black). The color codes for the orientations are the same as in Figs. 2 through 5.

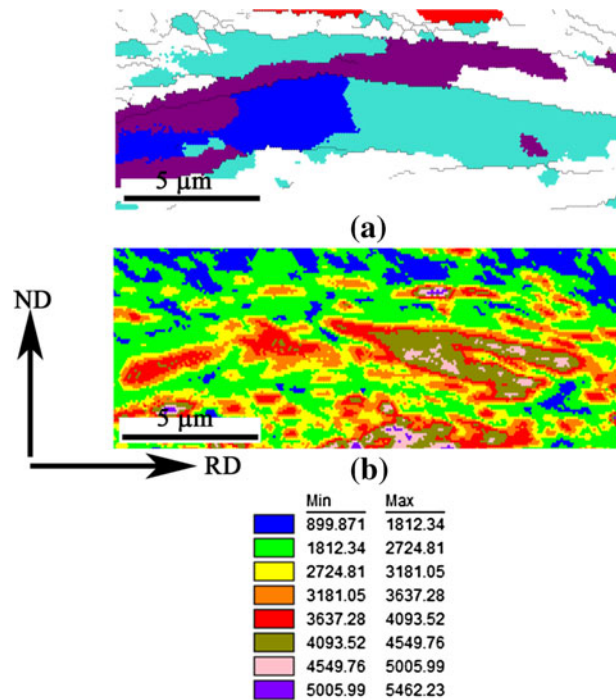


Fig. 9—(a) Orientation maps of cube-oriented regions of Fig. 4(b). Color codes for the orientations are the same as in Fig. 4(b). (b) is the corresponding IQ distribution map. Legends are the IQ values.

growth of grains of other orientations contributing to the observed weakening of the ND||[111] fiber texture.

The failure to observe the formation of strong cube texture in recrystallized cross-rolled Ni remains interesting from the mechanistic point of view. Merlini and Beck^[11] have explained the absence of cube texture in cross-rolled copper through the oriented growth model and discarded the role of oriented nucleation because cube regions exist in the deformed structure, but strong cube texture formation is not observed up on annealing. Strong preferential nucleation of near cube-oriented grains is not observed in the current study as well. However, the absence of preferential nucleation of cube grains leading to the absence of a strong final cube texture may be interpreted as a support to the oriented nucleation theory but in a negative sense. It is to be kept in view that internal structure of the cube bands and local misorientation environment are far more important factors than the mere presence of large cube-oriented regions in deformed microstructures as shown recently by one of the present authors.^[23] The preferential nucleation of cube grains is aided by the already recovered structure of the cube grains because of the special arrangement of gliding dislocations with orthogonal burgers vector.^[24] The substructure destabilization during cross rolling can affect the attainment of a recovered structure in near cube-oriented regions so crucial for early nucleation. Indirect evidence for this could be obtained from the IQ distribution map (Figure 9(b)) of the region surrounding the cube band of Figure 4(b), cropped and reproduced in Figure 9(a), which gives an indirect estimate of the distribution of stored energy. It may be clearly observed that the C^{TD}-

oriented regions (aqua) has much higher IQ than adjacent near C oriented regions (blue) indicating more recovered structure of the former. Incidentally, more C_{TD}-oriented grains are actually observed in the annealed materials as already discussed. Further, the cube-oriented regions are also observed at the vicinity of the locally sheared regions which can also play an important role because of their adverse impact on the nucleation and growth of cube grains.^[24,25] While the internal structure and misorientation environment appear as important factors, the current experimental results are not sufficient to fully understand the reasons for inhibition of nucleation of cube grains in heavily cross-rolled and annealed nickel. More direct studies are therefore felt necessary. Further transmission electron microscopy (TEM)-based investigations are necessary to study in detail the internal structure of the cube regions and local misorientation environment in cross-rolled nickel to clarify these issues.

V. CONCLUSIONS

The following major conclusions may be drawn from the current study:

- 1) The texture of heavily deformed cross-rolled nickel is characterized by the strong presence of B_S and B_SND components, which agrees well with the theoretical predictions.
- 2) The microtexture after low-temperature annealing at 673 K (400 °C) shows a ND||[111] fiber. The strongest orientation of the fiber, (445)[132̄38] is thought to originate from the twin formation of the TD-rotated cube component (027)⟨072⟩. This is also confirmed from the EBSD studies on early stages of recrystallization.
- 3) The twin formation is favored during low-temperature annealing supposedly because the reorientation due to twin formation can assist in overcoming the growth stagnation.
- 4) After high-temperature annealing at 1073 K (800 °C), the ND||[111] fiber is weakened. This agrees well with decreased twin-formation activity at higher annealing temperatures. The annealing texture at 1073 K (800 °C) is also found weak and rather diffused.
- 5) Preferential nucleation of near cube grains is not observed at early stages of recrystallization in cross-rolled nickel resulting in the formation of a weak cube texture. The internal structure and local misorientation environment of cube regions in cross-rolled nickel appear to be important factors for this behavior, but need to be investigated further in detail.

ACKNOWLEDGMENTS

The authors would like to thank Professor I. Samajdar, IIT Mumbai, India for providing access to the national facility for Texture-OIM (DST-IRPHA) at IIT Bombay,

India. Sincere thanks are also due to Professor N. Tsuji, Kyoto University, Japan for his kind permission to carry out the cross-rolling process in his laboratory. The travel support for visiting Kyoto University, Japan through DST–JSPS bilateral project (DST/INT/JSPS/P-114/2011) is gratefully acknowledged.

REFERENCES

1. R.D. Doherty: *Prog. Mater. Sci.*, 1997, vol. 42 (1–4), pp. 39–58.
2. J. Hirsch and K. Lucke: *Acta Metall.*, 1988, vol. 36 (11), pp. 2863–82.
3. T. Leffers and R.K. Ray: *Prog. Mater. Sci.*, 2009, vol. 54 (3), pp. 351–96.
4. R.K. Ray: *Acta Metall. Mater.*, 1995, vol. 43 (10), pp. 3861–72.
5. S. Suwas and A.K. Singh: *Mater. Sci. Eng. A*, 2003, vol. 356 (1–2), pp. 368–71.
6. X.Y. Kong, W.C. Liu, J. Li, and H. Yuan: *J. Alloy. Compd.*, 2010, vol. 491 (1–2), pp. 301–07.
7. D. Solas, S. Chhann, T. Baudin, and R. Penelle: *Mater. Sci. Forum*, 2010, vols. 636–637, pp. 538–43.
8. H. Tian, H. Suo, J. Zhou, M. Gao, L. Ma, H. Qiu, Z. Wang, M. Liu, D. Yuan, and Y. Wang: *Rare Met. Mater. Eng.*, 2012, vol. 41 (1), pp. 87–91.
9. C.Y. Chung: *Proceedings of the Eleventh International Conference on Textures of Materials*, 1996, pp. 711–16.
10. S. Suwas, A.K. Singh, K.N. Rao, and T. Singh: *Z. Metallkd.*, 2003, vol. 94 (12), pp. 1313–19.
11. A. Merlini and P.A. Beck: *Acta Metall.*, 1953, vol. 1 (5), pp. 598–606.
12. T. Öztürk: *Scripta Metall.*, 1988, vol. 22 (10), pp. 1611–16.
13. N.P. Gurao, S. Sethuraman, and S. Suwas: *Mater. Sci. Eng. A*, 2011, vol. 528 (25–26), pp. 7739–50.
14. S.H. Hong and D.N. Lee: *J. Eng. Mater. Technol. Trans. ASME*, 2002, vol. 124 (1), pp. 13–22.
15. R.D. Doherty, D.A. Hughes, F.J. Humphreys, J.J. Jonas, D.J. Jensen, M.E. Kassner, W.E. King, T.R. McNelley, H.J. McQueen, and A.D. Rollett: *Mater. Sci. Eng. A*, 1997, vol. 238 (2), pp. 219–74.
16. A. Goyal, M.P. Paranthaman, and U. Schoop: *MRS Bull.*, 2004, vol. 29 (8), pp. 552–61.
17. P.P. Bhattacharjee, R.K. Ray, and A. Upadhyaya: *J. Mater. Sci.*, 2007, vol. 42 (6), pp. 1984–2001.
18. P. Van Houtte: *Manual of MTM-FHM*, MTM-KU, Leuven, 1995.
19. R. Garg, N.P. Gurao, S. Ranganathan, and S. Suwas: *Philos. Mag.*, 2011, vol. 91 (32), pp. 4089–4108.
20. J. Savoie and J.J. Jonas: *Acta Metall. Mater.*, 1994, vol. 42 (12), pp. 4101–16.
21. L.S. Toth, J.J. Jonas, D. Daniel, and R.K. Ray: *Metall. Trans. A*, 1990, vol. 21A, pp. 2985–3000.
22. D.P. Field, L.T. Bradford, M.M. Nowell, and T.M. Lillo: *Acta Mater.*, 2007, vol. 55 (12), pp. 4233–41.
23. P.P. Bhattacharjee, Y. Takatsuji, Y. Miyajima, D. Terada, and N. Tsuji: *Metall. Mater. Trans. A*, 2012, vol. 43A, pp. 2442–52.
24. A.A. Ridha and W.B. Hutchinson: *Acta Metall.*, 1982, vol. 30 (10), pp. 1929–39.
25. P.P. Bhattacharjee, R.K. Ray, and N. Tsuji: *Acta Mater.*, 2009, vol. 57 (7), pp. 2166–79.